PLANT SCIENCE

CRISPR-Cas–mediated heritable chromosome fusions in *Arabidopsis*

Michelle Rönspies[1], Solmaz Khosravi[2†], Ondřej Helia[3,4], Alessandro Valisi[1], Jiří Fajkus[3,4], Miloslava Fojtová[3,4], Andreas Houben[2], Holger Puchta[1*]

The genome of *Arabidopsis thaliana* consists of 10 chromosomes. By inducing CRISPR-Cas–mediated breaks at subcentromeric and subtelomeric sequences, we fused entire chromosome arms, obtaining two eight-chromosome lines. In one line, both arms of chromosome 3 were fused to chromosome 1. In another line, the arms were transferred to chromosomes 1 and 5. Both chromosome number–reduced lines were fertile. Phenotypic and transcriptional analyses revealed no differences compared with wild-type plants. After crossing with the wild type, the progeny showed reduced fertility. The meiotic recombination patterns of the transferred chromosome arms were substantially changed. Directed chromosome number changes in plants may enable new breeding strategies, redefining linkage groups and establishing genetic barriers. Moreover, our data indicate that plants are highly robust to engineered karyotype changes.

The emergence of the CRISPR–CRISPR-associated protein (CRISPR-Cas) system has allowed scientists to induce double-strand breaks (DSBs) at almost any predefined position in the genome (*1*). In plants, this technique can be used for crop improvement by manipulating agronomically important traits (*2*–*4*). However, in addition to gene modifications, larger structural changes can also be induced. Using the CRISPR-Cas–based chromosome engineering technique, large chromosomal rearrangements such as inversions can be induced in plants (*5*–*10*). Inversions are known to modulate the recombination landscape along a chromosome by suppressing crossovers (COs) in the rearranged area (*11*–*16*). We were able to show the potential of inducing inversions for changing recombination patterns by both restoring CO rates in a previously CO-dead region (*6*) and excluding a substantial part of the *Arabidopsis* genome from meiotic recombination by inverting almost an entire chromosome (*10*).

In addition to inversions, chromosome fusions are also implicated in speciation through reproductive isolation because of the production of inviable gametes (*17*). As a proof of concept, we aimed to artificially reduce chromosome numbers by inducing chromosome fusions. Thus far, chromosome number changes have been achieved in a targeted manner in only a few other nonplant organisms (*18*–*20*).

Our results demonstrate the resilience of the plant genome toward massive restructuring, and our approach provides a unique opportunity for gaining further insights into speciation, genome evolution, and potential biotechnological applications.

[1]Joseph Gottlieb Kölreuter Institute for Plant Sciences - Molecular Biology, Karlsruhe Institute of Technology, Karlsruhe, Germany. [2]Leibniz Institute of Plant Genetics and Crop Plant Research Gatersleben, Seeland, Germany. [3]Mendel Centre for Plant Genomics and Proteomics, Central European Institute of Technology (CEITEC), Masaryk University, Brno, Czech Republic. [4]National Centre for Biomolecular Research, Faculty of Science, Masaryk University, Brno, Czech Republic. ***Corresponding author. Email: holger.puchta@kit.edu**
†Present address: Julius Kühn-Institut (JKI), Quedlinburg, Germany.

Creation of the eight-chromosome lines

Our approach required the introduction of two consecutively induced chromosome (arm) fusions in the form of reciprocal translocations between both arms of chromosome 3 and the ends of one or two receiving chromosomes. To obtain these rare events, we used our protocol for inducing megabyte-sized chromosomal rearrangements in *Arabidopsis* (*21*). Either the wild-type (WT) Col-0 (for line F8) or the *ku70* mutant (for line T8) were used as the genetic background. The *ku70* mutant was chosen because we had observed increased rearrangement frequencies in this line compared with WT in previous experiments because of the absence of the classical nonhomologous end joining DSB repair pathway (*5*, *22*). To ensure the production of heritable events, we combined the *Staphylococcus aureus* ortholog of Cas9 and the *Lachnospiraceae bacterium* variants ttLbCas12a or ttLbCas12a-I (*23*, *24*), optimized for plant use, with an egg cell–specific promoter (*25*). Using this setup, two DSBs were induced at the borders of the core centromere of chromosome 3 and near the telomere repeats of the respective receiver chromosomes (table S1). To create line F8 (Fig. 1A), the short arm of chromosome 3 was first transferred onto the long arm of chromosome 1, creating a telocentric and elongated chromosome. In the second step, the remaining arm of the telocentric chromosome was transferred onto the short arm of chromosome 1, resulting in one very large fusion chromosome. Line T8 (Fig. 1B) was generated by first transferring the short arm of chromosome 3 onto the long arm of chromosome 5 and then transferring the remaining arm of chromosome 3 from the telocentric chromosome onto the long arm of chromosome 1 in the second step, generating two elongated fusion chromosomes in the process. As a by-product of these approaches, the generation of a minichromosome was expected, consisting of the functional centromere of chromosome 3 and two short (~10 kb) telomere ends of either chromosome 1 (line F8) or chromosomes 1 and 5 (line T8), respectively. However, because of its small size and lack of essential genetic information (table S2), we expected that the minichromosome might get lost in the progeny because of segregation problems.

We first screened for plants in which the short arm of chromosome 3 was either translocated onto the end of the long arm of chromosome 1 (line F8) or that of chromosome 5 (line T8). One plant of line T8 and two plants of line F8 were found to carry the translocation heterozygously (tables S3 and S4). The recombinant T8 plant and one of the two positively identified F8 plants were chosen for further experiments and establishment of homozygosity. Homozygous plants were then subjected to a second round of chromosome engineering to transfer the remaining long arm of chromosome 3 onto the short arm (line F8) or long arm (line T8) of chromosome 1. For line F8, five lines were found to carry independent arm transfers (tables S3 and S4). When screening line T8 for the second arm transfer, four lines with independent arm transfer events were identified (tables S3 and S4). In two of these lines, Mendelian segregation of the arm transfer junction was detected, yielding homozygous eight-chromosome lines in the T_2 generation. In line F8, but not line T8, a junction indicative of the presence of the minichromosome (in the heterozygous state) could be detected, and in only one of three minichromosome-positive lines was the minichromosome inherited. By screening three different seed batches of this line, the minichromosome junction could be detected in eight, 10, or 14 of 80 screened plants, respectively. This indicates that the minichromosome is rapidly lost during propagation because it apparently does not contain any essential genetic information (table S2). To establish lines F8 and T8, one minichromosome-negative line each was chosen for further experiments and homozygous mutants were propagated. All newly formed translocation junctions that were amplified by polymerase chain reaction and analyzed by Sanger sequencing exhibited InDels around the ligation sites (fig. S1). In line T8 (*ku70* genetic background), deletion repair patterns likely resulting from microhomology-mediated end joining repair could be observed. Furthermore, the translocation and fusion events generated in both

Downloaded from https://www.science.org at KIT Library on November 20, 2025

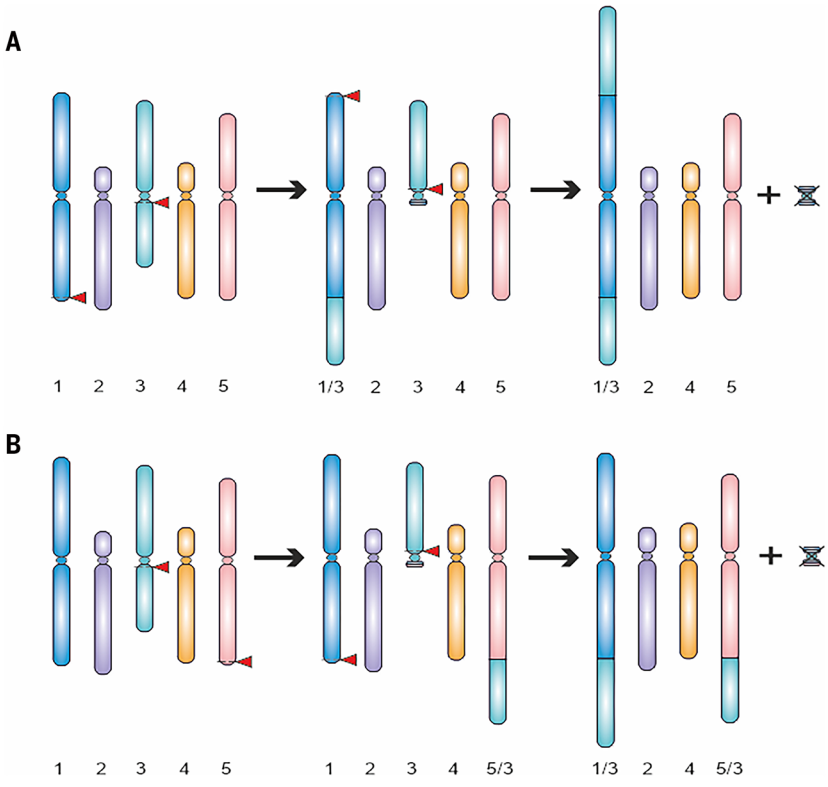

Fig. 1. Schematic overview of the generation of the two eight-chromosome lines F8 and T8. Schematic overview of the induced chromosome arm translocations of chromosome 3 in lines F8 and T8, leading to the creation of an eight-chromosome karyotype. As a by-product, the generation of a minichromosome was expected, consisting of the functional centromere of chromosome 3 and two short (~10 kb) telomere ends of chromosome 1 or chromosomes 1 and 5. However, because of its small size and lack of essential genetic information, we expected that the minichromosome might get lost in the progeny. Red triangles and dashed lines indicate the location of CRISPR-Cas–induced DSBs. (**A**) Schematic overview of the induced chromosome arm translocations of chromosome 3 in line F8. First, two DSBs were induced at the border of the core centromere of chromosome 3 and near the telomere sequences of chromosome 1. This resulted in the transfer of the short arm of chromosome 3 onto the long arm of chromosome 1, creating a telocentric and elongated chromosome through a reciprocal translocation in the process. Next, two DSBs were induced at the border of the core centromere of chromosome 3 on the remaining arm and near the remaining telomere sequences of chromosome 1. This resulted in the transfer of the remaining long arm of chromosome 3 onto the short arm of chromosome 1, creating a fusion chromosome of chromosomes 1 and 3. (**B**) Schematic overview of the induced chromosome arm translocations of chromosome 3 in line T8. First, two DSBs were induced at the border of the core centromere of chromosome 3 and near the telomere sequences of chromosome 5. This resulted in the transfer of the short arm of chromosome 3 onto the long arm of chromosome 5, creating a telocentric and elongated chromosome through a reciprocal translocation in the process. Next, two DSBs were induced at the border of the core centromere of chromosome 3 on the remaining arm and near the telomere sequences of chromosome 1. This resulted in the transfer of the remaining long arm of chromosome 3 onto the long arm of chromosome 1 in inverted orientation, creating another elongated chromosome in the process.

eight-chromosome lines were validated by fluorescence in situ hybridization (FISH) using chromosomal segment–specific probes (Fig. 2, A to D, and table S5). The loss of the centromeric minichromosomes formed from chromosome 3 and the reduction of the chromosome numbers to eight were confirmed in both lines by 4′,6-diamidino-2-phenylindole (DAPI) staining of mitotic chromosomes (Fig. 2E) and immunostaining of interphase nuclei with a centromere-specific CENH3 antibody (Fig. 2F). A maximum of eight CENH3 signals were detected in both engineered lines; by contrast, most nuclei showed up to 10 signals in WT Col-0 nuclei (Fig. 2F). To further confirm the genomic structure and to rule out the occurrence of major off-target rearrangements, both homozygous eight-chromosome lines were sequenced using the PacBio HiFi sequencing method. The expected junctions were verified, and no major off-target chromosomal rearrangements were detected (figs. S2 and S3 and data S1).

Gene expression and phenotype remain unaffected by the karyotype changes

Next, the effect of the chromosome fusions on gene expression was determined. Compared with WT Col-0, only 0.3% (n = 88) and 0.5% (n = 151) of total genes (N = 27,000) in line F8 and line T8, respectively, displayed significant differential expression (fig. S4). In both lines, the differentially expressed genes (DEGs) were distributed over the entire genome and there was little overlap between them (fig. S4). Gene Ontology term analysis of the DEGs mostly showed their enrichment in metabolism pathways and no association with DNA repair mechanisms (fig. S5). The identified DEGs were not located near the chromosomal fusion sites, ruling out a chromosome position effect on gene expression.

In addition, the macroscopic effects of the chromosome number reductions were analyzed in lines T8 and F8. Phenotypes were monitored across multiple developmental stages, from late seedlings up to 22 days after sowing, with a total of seven scanning sessions (fig. S6A). The PlantScreen system measured 10 morphological parameters ranging from basic traits such as a raw area or perimeter to more complex traits such as compactness or slenderness of leaves (*26*). Phenotypic data from each scan were analyzed by principal components analysis (PCA) (fig. S7 and data S2). To enable an integrated comparison of developmental phenotypes, PCA was performed across all time points (Fig. 3A and data S2). The first two principal components (PC1 and PC2) explained 71.4 and 17.4% of the total variation, respectively. For a more comprehensive view of phenotypic variation, PCA results were visualized in three dimensions (3D) by including PC3, which accounted for 5.8% of the total variation (fig. S8 and data S2). Next, root morphology was assessed by measuring the primary root length of seedlings (fig. S6B and data S2), revealing no significant differences between the engineered and Col-0 lines. Seed phenotyping analysis further confirmed these results (fig. S9 and data S2). These data clearly demonstrate that the eight-chromosome plants retained a WT-like phenotype throughout all developmental phases.

Fertility of the eight-chromosome lines

We assessed the effect of the chromosome fusions on the fertility of homozygous and heterozygous mutant plants compared with WT Col-0 plants by counting the number of seeds per silique. In both lines, the total seed number did not differ significantly between homozygous mutant and WT plants, so haploid gametes of both eight-chromosome karyotypes seem to be fully fertile (Fig. 3, B and C, and data S2). In the case of line F8 (Fig. 3B), we detected a decrease in the seed number per silique by ~60% in heterozygous plants compared with WT plants and the homozygous mutant. In line T8, the seed number of heterozygous plants was reduced by ~75% compared with WT plants and the homozygous mutant (Fig. 3C). We speculated that meiotic pairing defects of the fusion chromosome with *Arabidopsis* WT chromosomes might lead to partial infertility. In line F8, both WT chromosomes 3 and 1 must pair simultaneously with the fused chromosome to enable proper

Downloaded from https://www.science.org at KIT Library on November 20, 2025

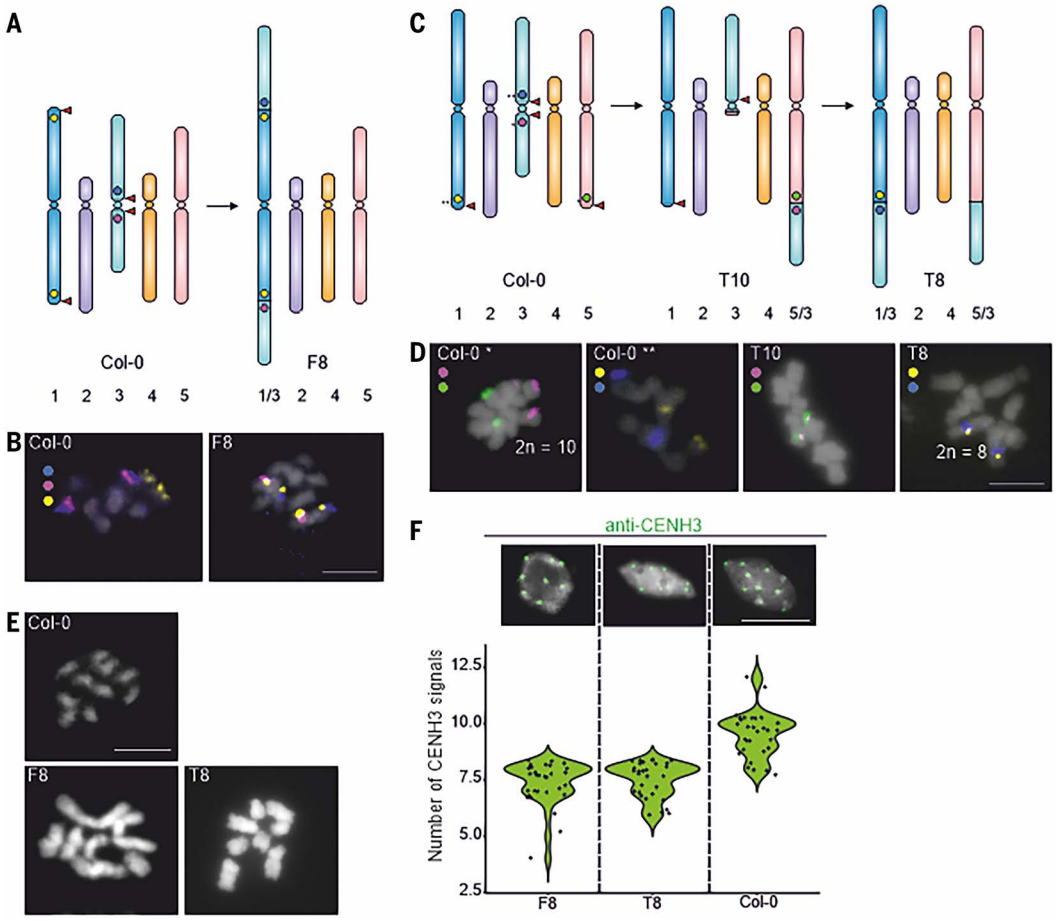

Fig. 2. Confirmation of the eight-chromosome lines by FISH, DAPI staining, and CENH3 immunostaining. (**A**) Schematic overview showing placement of the FISH probe combinations in WT Col-0 (left) and line F8 (right). Red triangles and dashed lines indicate the location of CRISPR-Cas–induced DSBs. The positions of FISH probes are indicated by colored circles. (**B**) FISH of mitotic Col-0 and F8 chromosomes with the probe combination of yellow, dark blue, and magenta (table S5). On Col-0 chromosomes, blue and magenta signals are located on chromosome 3 and the yellow signal is located on chromosome 1; in line F8, blue and magenta signals colocalize with yellow on the same fusion chromosome. Chromatin was counterstained with DAPI (gray). Scale bar, 10 μm. (**C**) Schematic overview showing placement of the FISH probe combinations in Col-0 (left), intermediate line T10 harboring the first chromosome arm translocation (middle), and line T8 (right). (**D**) FISH of mitotic Col-0, T10, and T8 mitotic chromosomes. In Col-0 (*), the probe combination magenta and green (table S5) is located on separate chromosomes 3 and 5, and in line T10, colocalization of the probes confirms the first translocation event between chromosomes 3 and 5. In Col-0 (**), the probe combination yellow and dark blue (table S5) is located on separate chromosomes 1 and the remaining arm of chromosome 3, and in line T8, colocalization of the probes confirms the second chromosome arm transfer. Chromatin was counterstained with DAPI (gray). Scale bar, 10 μm. (**E**) DAPI-stained mitotic chromosomes of lines F8, T8, and Col-0. Scale bar, 10 μm. (**F**) Anti-CENH3–labeled interphase nuclei of lines F8, T8, and Col-0. The rare occurrence of nuclei with CENH3 signals >10 is explained by the partial separation of sister chromatids (*46*). At least 30 nuclei were analyzed per line.

segregation and thus viable gametes. To visualize the meiotic behavior of line F8, DAPI staining was performed on meiotic metaphase I chromosome spreads prepared from the hybrid plants between line F8 and WT. As expected, we detected three bivalents and one trivalent. By contrast, WT plants formed five bivalents (Fig. 3, D to F).

Chromosome fusions change recombination patterns in hybrids

To elucidate how the chromosome fusions influence meiotic recombination in hybrids, both homozygous engineered eight-chromosome lines were crossed with the *Arabidopsis* ecotype Landsberg erecta (Ler-1) harboring the WT 10-chromosome set. Subsequently, F_1 seeds were harvested and propagated to obtain F_2 seeds. The recombination frequency was determined by analyzing 400 plants per line that were grown from the F_2 seeds. As a control, 400 plants of the progeny of crosses between WT Col-0 and Ler-1 (control for line F8) or *ku70* and Ler-1 (control for line T8), respectively, were analyzed. Using a TaqMan single-nucleotide polymorphism (SNP) genotyping assay, we selected SNP markers approximately every 2 Mb on the fused chromosomes to detect marker changes between Col-0 and Ler-1 alleles (tables S4 and S6). First, the presence or absence of a marker change was analyzed in each sample in each marker interval. Then, on the basis of the total number of marker changes in each marker interval, the recombination frequency was determined (Fig. 4 and data S2). In both lines, the chromosome fusion sites were depleted of COs compared with the respective chromosome areas in the control. At the same time, the recombination pattern detected in all translocated arms of chromosome 3 was inverted, shifting the COs from the fusion sites toward the telomeric ends. Conversely, the recombination pattern in the respective fusion partners, chromosome 1 or chromosome 5, was either unchanged or only slightly different from that in the corresponding WT control. In the long arm of chromosome 4, which was analyzed as another control, no difference in recombination pattern was observed between the engineered lines and the WT. Therefore, the chromosome arm transfers influenced the recombination landscape specifically at the fusion sites and in the fused arms.

Downloaded from https://www.science.org at KIT Library on November 20, 2025

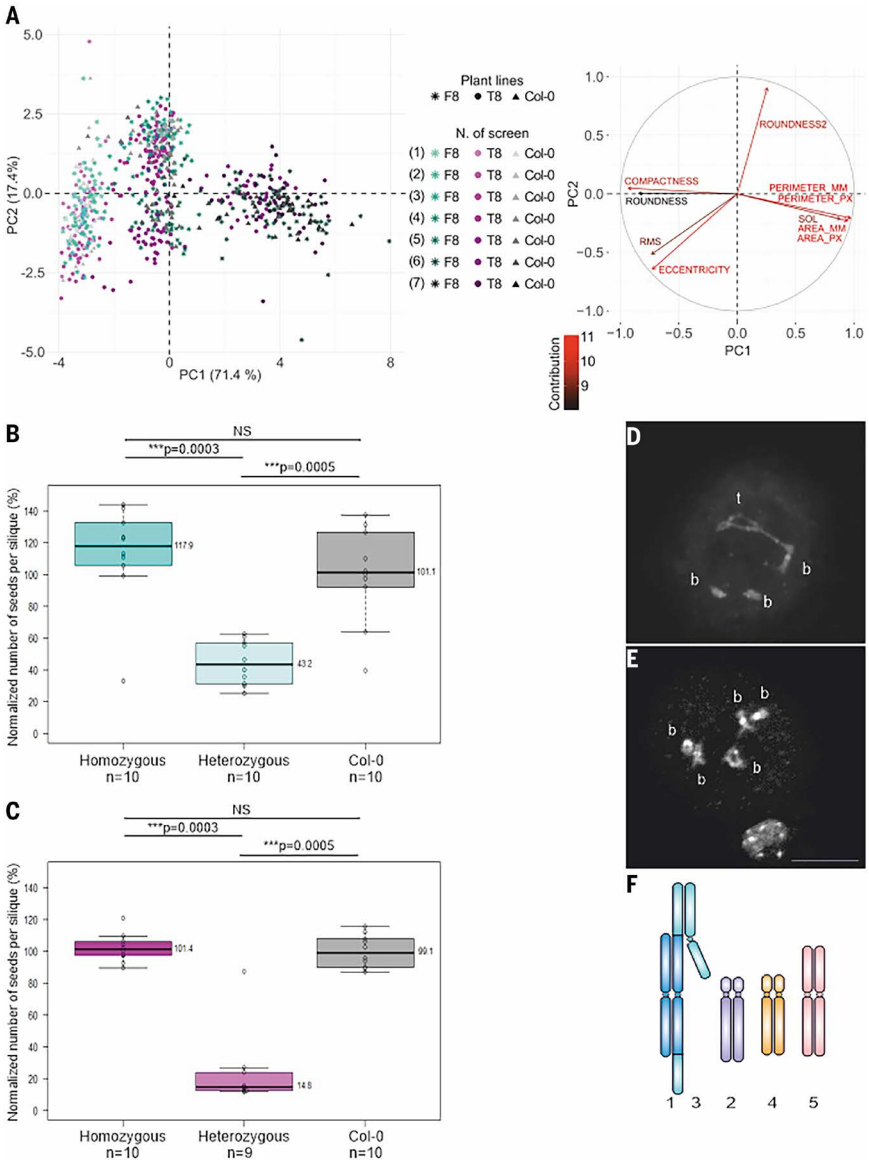

Fig. 3. Phenotypic and fertility analyses of lines F8 and T8 and meiotic chromosome Ppairing behavior of the eight-chromosome line F8. (**A**) PCA plot (left) and bi-plot (right) integrating phenotypic data of all seven scanned developmental stages. Arrows indicate the contribution of the individual morphological traits to the principal components (the longer the arrow, the higher the contribution). For each phenotype scan, $n \geq 30$ independent biological replicates for F8 and T8 and $n \geq 15$ for Col-0. For a more comprehensive view of phenotypic variation, PCA results were visualized in 3D by including PC3, which accounted for 5.8% of the total variation (fig. S8). (**B** and **C**) Homozygous, heterozygous, and Col-0 WT (Col) plants were randomly selected for fertility analysis ($n = 9$ or 10). Ten siliques per plant were randomly selected, and the number of seeds per silique was counted. The data were normalized to the mean seed count of Col-0, which was set to 100%. The boxplot shows the nine or 10 independent biological replicates for each genotype. The middle line represents the median, box edges represent the first and third quartiles, and whiskers extend to the minimum and maximum values. Individual data points are represented as open circles. The median values are indicated next to the middle line of each boxplot. *P* values were calculated using a two-sided Mann-Whitney *U* test (***$P < 0.001$; NS, not significant). (B) Fertility analysis of homozygous and heterozygous plants of line F8 and WT Col-0 plants. The seed number of the heterozygous plants was significantly reduced, by 56 and 61%, compared with Col-0 and homozygous plants, respectively. The seed number of homozygous and Col-0 plants did not differ significantly. (C) Fertility analysis of homozygous and heterozygous plants of line T8 and WT Col-0 plants. The seed number of the heterozygous plants was significantly reduced, by 76%, compared with Col-0 and homozygous plants. The seed number of homozygous and Col-0 plants did not differ significantly. (**D** and **E**) Meiotic chromosome pairing behavior of hybrids of the eight-chromosome line F8 and Col-0 (D) and Col-0 (E). The F8 × Col-0 hybrid shows the formation of one trivalent (marked by "t") plus three bivalents (marked by "b"). (E) Metaphase I cell of Col-0 showing five bivalents. Chromatin was counterstained with DAPI (gray). Scale bar, 10 μm. (**F**) Scheme of the formation of one trivalent plus three bivalents in the F8 × Col-0 hybrid plant.

Discussion

With the advance of large-scale sequencing and chromosome painting technologies, it has become clear that chromosome fusion events regularly take place in the course of genome evolution (*27*–*29*). The development of the CRISPR-Cas–mediated chromosome engineering technology has now allowed us to fuse chromosomes in a predefined way and thus to induce chromosome number reductions in plants in a targeted manner. The eight-chromosome *Arabidopsis* lines exhibited a completely WT-like phenotype during development and only minimal transcriptomic changes (*30*). Furthermore, the identified DEGs were not involved in DNA repair, indicating regular genome stability given that no persistent DNA damage signaling took place in these lines (*31*). These results also strongly resemble those obtained when analyzing two 5- and 7.5-Mb CRISPR-Cas–induced chromosomal inversions (*7*) and 0.5-Mb translocations (*30*) regarding their effect on epigenetic landscape and gene expression. Taken together, these results demonstrate the robustness of the plant genome toward substantial chromosomal restructuring.

However, chromosome fusions may have consequences for the evolution of species because they often coincide with reduced fertility in hybrids. Crossing with WT karyotypes results in heterozygotes that, because of disturbed meiotic pairing of the homologous chromosomes, display the generation of imbalanced gametes (*17*). We found a reduction in fertility of ~60% in line F8 and ~85% in line T8 compared with WT plants. We anticipate that with further structural chromosome changes, reproductive isolation between engineered and WT *Arabidopsis* plants will be achievable. In addition, using such a strategy, it should be possible to contain crops genetically and prevent outcrossing with wild relatives.

In two studies of haploid yeast, substantial chromosome number reductions were achieved by inducing consecutive chromosome fusions, leading to a reduction of the chromosome number from 16 to one and two chromosomes (*18*, *19*). In another study, the first chromosome fusions in mammals were achieved by editing haploid embryonic mice stem cells, resulting in the generation of animals with 19 instead of 20 pairs of chromosomes by fusing the two largest mouse chromosomes 1 and 2 as well as the two medium-sized chromosomes 4 and 5 (*20*). In all three studies, no major growth defects were detected; however, in contrast to our study, varying degrees of fertility impairments were observed.

In our experiments, the observed reduced fertility in heterozygotes indicated that meiotic segregation was affected by the presence of the chromosome fusions. Because successful chromosome pairing is a prerequisite for balanced segregation of the haploid chromosome sets during meiosis, aberrant gametes might have been produced due to the missegregation of the nonaligned engineered and WT chromosomes. In this situation, trivalents are likely to form, a complex and error-prone process, because the fused arms of chromosome 3 can pair with two different WT chromosomes at the same

Downloaded from https://www.science.org at KIT Library on November 20, 2025

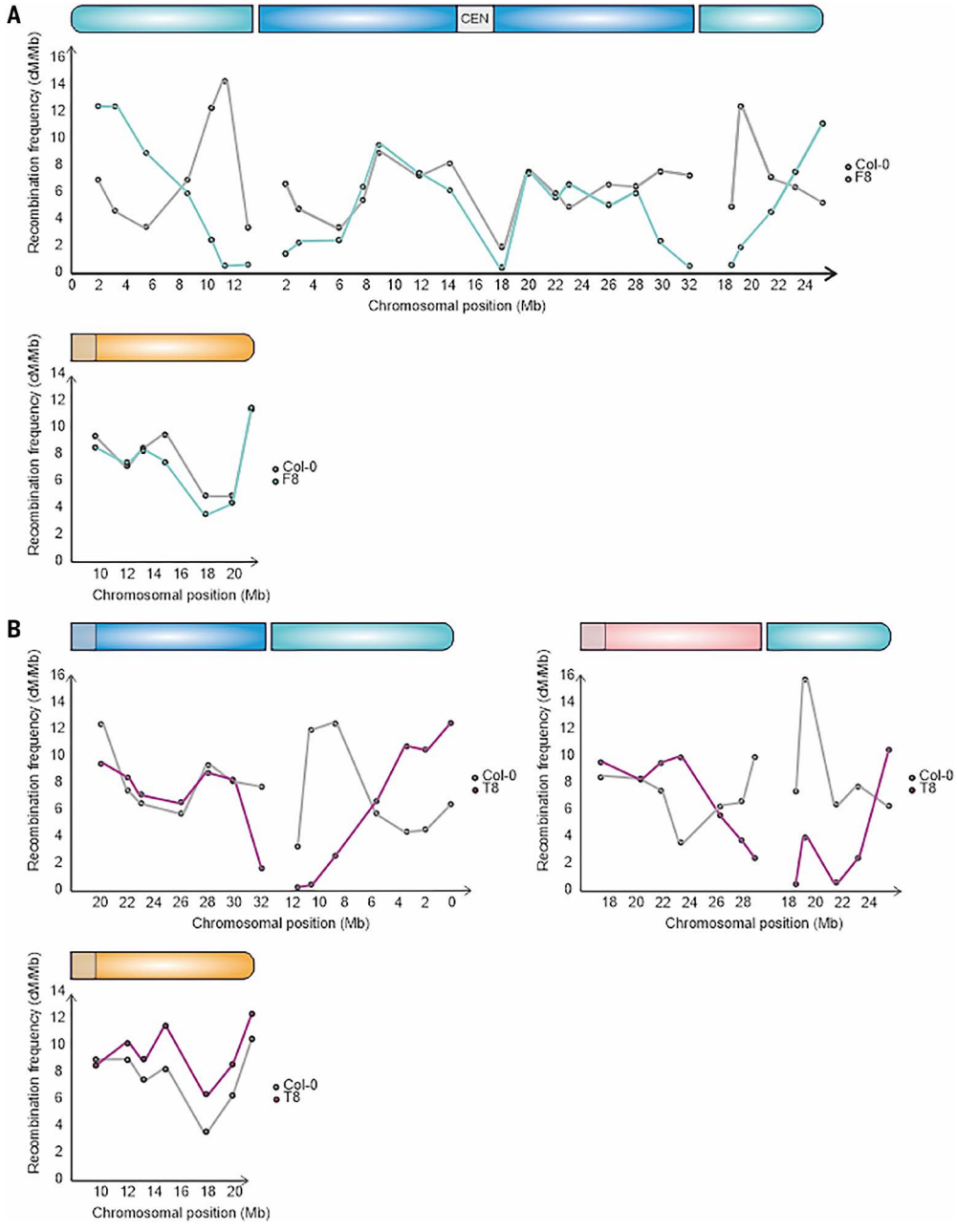

Fig. 4. Recombination frequency on the fusion chromosome arms and long arm of chromosome 4. (**A**) Recombination frequency on the fusion chromosome 1/3 (top) and the long arm of chromosome 4 (bottom) as a control in line F8 was determined by SNP-based genotyping of 400 plants (independent biological replicates) of the offspring of the F8 × Ler-1 line and the Col-0 × Ler-1 control. The recombination frequency is presented in cM/Mb. Chromosomal areas that were not analyzed are grayed out. (**B**) Recombination frequency on the arms of the fusion chromosome 1/3 (left) and 5/3 (right) and the long arm of chromosome 4 (bottom) as a control in line T8 was determined by SNP-based genotyping of 400 plants (independent biological replicates) of the offspring of the T8 × Ler-1 line and the *ku70* × Ler-1 control. Chromosomal areas that were not analyzed are grayed out. In both lines, we detected an inverted recombination pattern in the two translocated arms of chromosome 3, shifting the CO from the fusion sites toward the telomeric ends. At the same time, the chromosome fusions sites were depleted of COs compared with the respective chromosome areas in the control. The recombination pattern in the fusion partners, chromosome 1 and/or 5, did not differ from the pattern in the control.

time. Indeed, we were able to identify such a structure during meiosis (Fig. 4C). In addition to segregation, the natural recombination reaction itself might have also been influenced by the chromosome structure changes. In the offspring of crosses between the engineered eight-chromosome lines and Ler-1 (with a 10-chromosome set), we observed in both analyzed lines that the fusion sites were depleted of COs compared with the respective chromosome areas in the control, indicating impairments in homolog pairing close to the newly added heterologies. In both analyzed lines, the recombination pattern detected in all translocated arms of chromosome 3 was inverted, shifting the COs from the fusion sites toward the subtelomeric ends. These results could indicate that the complete formation of the synaptonemal complex during meiosis, a prerequisite for CO formation (*32*), was inhibited close to the fusion sites. The observed increase in CO frequencies toward the chromosome ends could be caused by a compensation mechanism, accounting for the reduced CO frequencies at the fusion sites to allow for the obligate CO necessary for proper segregation of the chromatids (*32*, *33*). For plant breeders, it will be of particular interest that by inducing large chromosomal translocations, the recombination landscape can be changed, both by reducing CO numbers near the newly brought-in heterologous regions and at the same time by enhancing COs in the subtelomeric parts of the elongated chromosome arms. Future application of the eight-chromosome lines in combination with meiotic mutants might be helpful to test the interplay between chromosome number reduction and interference-sensitive versus interference-insensitive CO pathways and also to test the coarsening model (*34*).

The applied chromosome fusion approach can also help to answer other basic research questions. For example, what are the minimum and maximum lengths of *Arabidopsis* chromosomes required to still be inherited? Minichromosomes are often lost during meiosis (*35*). In our lines, the minichromosomes were not carrying essential genes, so it is likely that there was no selective pressure to inherit them over several generations. However, we should soon be able to define the minimal size of functional *Arabidopsis* chromosomes by inducing translocations of different sizes (*36*). Generally, minichromosomes have considerable potential for breeding applications because they can be used as vectors for stacking and transferring many genes, such as genes associated with increased nutritional value, pest resistance, or tolerance to abiotic stress (*37*). Because they segregate independently of the other native chromosomes, linkage drag can be avoided. For the same reason, CRISPR-Cas

Downloaded from https://www.science.org at KIT Library on November 20, 2025

editing components could be placed on minichromosomes and later easily eliminated from the genome by back-crossing to achieve transgene-free lines (*38*).

An upper limit on chromosome size has been suggested by studying artificially increased chromosome arms in *Vicia faba* and barley (*39*, *40*). Those studies indicated that the chromosome arms must not exceed half of the average length of the spindle axis at telophase to avoid truncation of the nonseparated sister chromatids by the newly forming cell wall, causing a loss of genetic information. In our study, all obtained elongated chromosome arms still adhered to this proposed length limit. Future experiments using chromosome engineering could help to illuminate whether the proposed length limit can also be confirmed in *Arabidopsis*.

Artificially induced chromosome fission has been achieved in plants (*41*, *42*). A synthetic centromere was inserted into chromosome 4 of maize, making it a functional dicentric chromosome. Random chromosome breakage during segregation resulted in a line harboring a chromosome number of 22 instead of 20. The resulting plants showed no phenotypic deviation or growth defects and reproduced normally with 20-chromosome lines. By combining this approach with CRISPR-Cas–mediated chromosome engineering, one should be able to break up chromosomes at the desired position.

Our study demonstrates that by using CRISPR-Cas, we can now change the karyotype of plants in a predefined way. CRISPR-Cas–mediated chromosome number changes should be applicable to crops despite their larger and more complex genomes. In our experiments in *Arabidopsis*, we obtained translocation frequencies of complete chromosome arms of ~1 of 1000 tested plants (table S3). Because large intrachromosomal rearrangements have already been achieved in crops such as rice and maize (*8*, *9*) at frequencies similar to those observed in *Arabidopsis* (*6*, *10*), obtaining chromosome fusions in crops should not pose a significant obstacle if efficient plant transformation and screening protocols are used. Applying directed karyotype engineering will also allow us to mimic evolution, explore chromosome length limits, or achieve artificial reproductive isolation in the near future.

REFERENCES AND NOTES

1. J. Y. Wang, J. A. Doudna, *Science* **379**, eadd8643 (2023).
2. F. Wolter, P. Schindele, H. Puchta, *BMC Plant Biol.* **19**, 176 (2019).
3. B. Li, C. Sun, J. Li, C. Gao, *Nat. Rev. Genet.* **25**, 603–622 (2024).
4. A. Tuncel, C. Pan, J. S. Clem, D. Liu, Y. Qi, *Nat. Rev. Mol. Cell Biol.* **26**, 419–441 (2025).
5. N. Beying, C. Schmidt, M. Pacher, A. Houben, H. Puchta, *Nat. Plants* **6**, 638–645 (2020).
6. C. Schmidt *et al.*, *Nat. Commun.* **11**, 4418 (2020).
7. S. Khosravi *et al.*, *New Phytol.* **245**, 2527–2539 (2025).
8. C. Schwartz *et al.*, *Nat. Plants* **6**, 1427–1431 (2020).
9. Y. Lu *et al.*, *Nat. Plants* **7**, 1445–1452 (2021).
10. M. Rönspies *et al.*, *Nat. Plants* **8**, 1153–1159 (2022).
11. A. H. Sturtevant, *Proc. Natl. Acad. Sci. U.S.A.* **7**, 235–237 (1921).
12. K. N. Crown, D. E. Miller, J. Sekelsky, R. S. Hawley, *Curr. Biol.* **28**, 2984–2990.e3 (2018).
13. K. Huang, L. H. Rieseberg, *Front. Plant Sci.* **11**, 296 (2020).
14. M. Kirkpatrick, N. Barton, *Genetics* **173**, 419–434 (2006).
15. J. M. Coughlan, J. H. Willis, *Mol. Ecol.* **28**, 1343–1357 (2019).
16. D. E. Miller, K. R. Cook, R. S. Hawley, *PLOS Genet.* **15**, e1008421 (2019).
17. J. M. de Vos, H. Augustijnen, L. Bätscher, K. Lucek, *Philos. Trans. R. Soc. Lond. B Biol. Sci.* **375**, 20190539 (2020).
18. J. Luo, X. Sun, B. P. Cormack, J. D. Boeke, *Nature* **560**, 392–396 (2018).
19. Y. Shao *et al.*, *Nature* **560**, 331–335 (2018).
20. L.-B. Wang *et al.*, *Science* **377**, 967–975 (2022).
21. M. Rönspies, P. Schindele, R. Wetzel, H. Puchta, *Nat. Protoc.* **17**, 1332–1358 (2022).
22. C. Schmidt, M. Pacher, H. Puchta, *Plant J.* **98**, 577–589 (2019).
23. P. Schindele, H. Puchta, *Plant Biotechnol. J.* **18**, 1118–1120 (2020).
24. P. Schindele *et al.*, *Plant Biotechnol. J.* **21**, 457–459 (2023).
25. F. Wolter, J. Klemm, H. Puchta, *Plant J.* **94**, 735–746 (2018).
26. M. Pavicic *et al.*, *Front. Plant Sci.* **8**, 416 (2017).
27. F. Yu *et al.*, *New Phytol.* **233**, 1953–1965 (2022).
28. P. G. Hofstatter *et al.*, *Cell* **185**, 3153–3168.e18 (2022).
29. H. Lewis, *Evolution* **7**, 102–109 (1953).
30. O. Helia *et al.*, *Plant J.* **121**, e70024 (2025).
31. I.-P. Chen, U. Haehnel, L. Altschmied, I. Schubert, H. Puchta, *Plant J.* **35**, 771–786 (2003).
32. D. Zickler, N. Kleckner, *Cold Spring Harb. Perspect. Biol.* **7**, a016626 (2015).
33. N. M. Pazhayam, C. A. Turcotte, J. Sekelsky, *Front. Cell Dev. Biol.* **9**, 681123 (2021).
34. J. A. Fozard, C. Morgan, M. Howard, *eLife* **12**, e79408 (2023).
35. I. Schubert, *Cytogenet. Cell Genet.* **93**, 175–181 (2001).
36. H. Puchta, A. Houben, *New Phytol.* **241**, 541–552 (2024).
37. J. A. Birchler *et al.*, *Plant J.* **120**, 2356–2366 (2024).
38. J. A. Birchler, N. D. Graham, N. C. Swyers, J. P. Cody, M. E. McCaw, *Curr. Opin. Biotechnol.* **37**, 135–142 (2016).
39. I. Schubert, J. L. Oud, *Cell* **88**, 515–520 (1997).
40. S. Hudakova, G. Künzel, T. R. Endo, I. Schubert, *Cytogenet. Genome Res.* **98**, 101–107 (2002).
41. Y. Zeng, M. Wang, J. I. Gent, R. K. Dawe, *Sci. Adv.* **11**, eadw3433 (2025).
42. R. K. Dawe *et al.*, *Nat. Plants* **9**, 433–441 (2023).
43. European Molecular Biology Laboratory, "European Nucleotide Archive" (EMBL-EBI, 2025); https://www.ebi.ac.uk/ena/browser/view/PRJEB89813.
44. National Center for Biotechnology Information, "PacBio Hifi reads from Arabidopsis thaliana 8-chromosome line" (NCBI, 2011); https://www.ncbi.nlm.nih.gov/bioproject/PRJNA1267949/.
45. AVinJKIP, AVinJKIP/8-chromosome-lines-Arabidopsis-thaliana-: CRISPR/Cas-mediated heritable chromosome fusions in Arabidopsis, version #chromsome_engineering, Zenodo (2025); https://doi.org/10.5281/zenodo.17185110.
46. V. Schubert *et al.*, *Genetics* **172**, 467–475 (2006).

ACKNOWLEDGMENTS

We thank J. Baumann, N. Schäfter, L. E. Rothenberger, C. Brechtel, A. Hamidi, O. Weiss and K. Kumke for excellent technical assistance in performing experiments; M. Cuacos for support with microscopy; A. Fiebeg for data submission; and J. J. Szymanski for network analysis advice. Additionally, the authors acknowledge the support of the Freiburg Galaxy Team, Bioinformatics, University of Freiburg (Germany) funded by the German Federal Ministry of Education and Research BMBF grant 031 A538A de.NBI-RBC and the Ministry of Science, Research and the Arts Baden-Württemberg (MWK) within the framework of LIBIS/de.NBI Freiburg. The Core Facility Plant Sciences, CEITEC Masaryk University, and Labdeers company (www.labdeers.com) are gratefully acknowledged for the support in obtaining scientific data presented in this paper. **Funding:** This work was supported by Reinhard Koselleck Project Pu137/24-1, Deutsche Forschungsgemeinschaft (H.P.); EpiChrom (031B1220B), BMBF (H.P. and A.H.); Czech Science Foundation project 22-04364S (M.F. and O.H.); and Toward Next GENeration Crops, reg. no. CZ.02.01.01/00/22_008/0004581, ERDF Programme Johannes Amos Comenius (M.F. and J.F.). **Author contributions:** Conceptualization: M.R., S.K., O.H., J.F., M.F., A.H., H.P.; Funding acquisition: J.F., M.F., A.H., H.P.; Investigation: M.R., S.K., O.H., A.V.; Methodology: M.R., S.K., O.H., A.V.; Visualization: M.R., S.K., O.H., A.V.; Writing – original draft: M.R., S.K., O.H., A.V., J.F., M.F., A.H., H.P.; Writing – review & editing: M.R., S.K., O.H., A.V., J.F., M.F., A.H., H.P. **Competing interests:** The authors declare no competing interests. **Data and materials availability:** All data are available in the main text or the supplementary materials or have been deposited into the following repositories. RNA-sequencing raw sequence reads are available from the European Nucleotide Archive (ENA) under accession number PRJEB89813 (*43*). PacBio raw sequence reads and genome assemblies are available from the NCBI Sequence Read Archive (SRA) and NCBI GenBank under BioProject number PRJNA1267949 (*44*). Custom Python scripts are available through Zenodo (*45*). **License information:** Copyright © 2025 the authors, some rights reserved; exclusive licensee American Association for the Advancement of Science. No claim to original US government works. https://www.science.org/about/science-licenses-journal-article-reuse

SUPPLEMENTARY MATERIALS

science.org/doi/10.1126/science.adz8505
Materials and Methods; Figs. S1 to S9; Tables S1 to S6; References (*47*–*72*); MDAR Reproducibility Checklist; Data S1 to S4

Submitted 17 June 2025; accepted 29 September 2025

10.1126/science.adz8505

Downloaded from https://www.science.org at KIT Library on November 20, 2025